Inorganic Chemistry

pubs.acs.org/IC

March 14, 2022 • Volume 61, Number 10

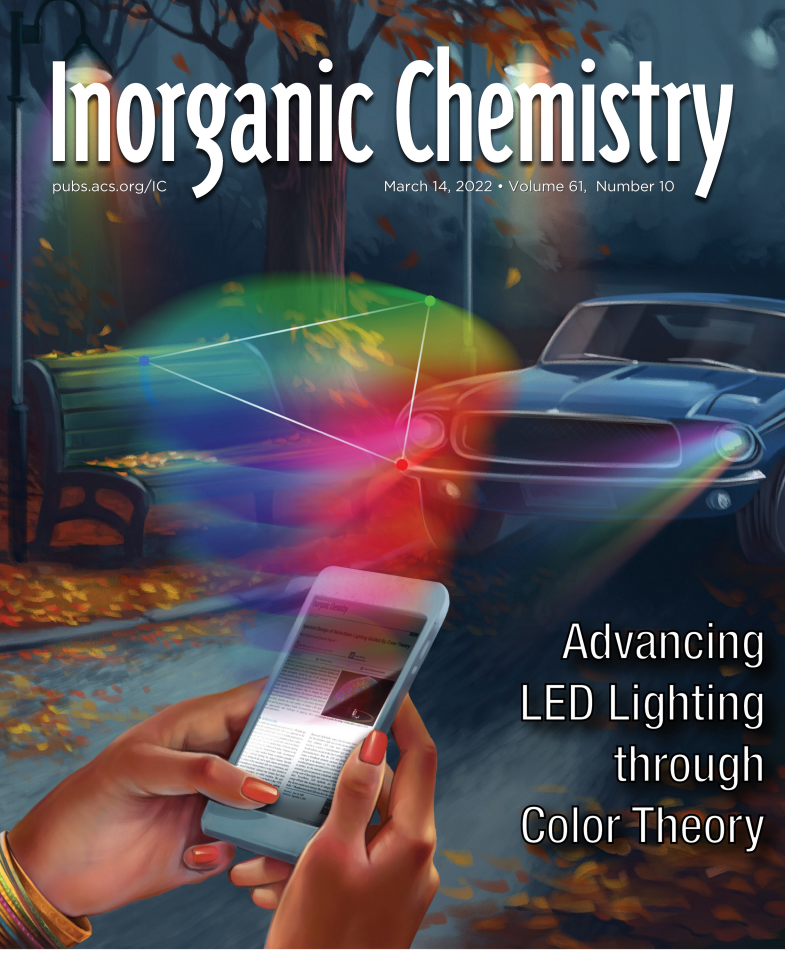

Advancing LED Lighting through Color Theory

ACS Publications
Most Trusted. Most Cited. Most Read.

www.acs.org

Inorganic Chemistry

pubs.acs.org/IC

Viewpoint

Spectral Design of Phosphor-Converted LED Lighting Guided by Color Theory

Shruti Hariyani and Jakoah Brgoch*

Cite This: *Inorg. Chem.* 2022, 61, 4205−4218

Read Online

ACCESS | Metrics & More | Article Recommendations

ABSTRACT: In the race to develop new luminescent materials for the next generation of light-emitting-diode (LED)-based solid-state lighting and display applications, it is often forgotten that color theory and human perception should be some of the principal factors guiding materials design. In this Viewpoint, we explore some of the antiquated colorimetrics established originally for incandescent and fluorescent lighting and discuss how they are still widely applied in the literature today to interpret the color quality of luminescent materials, like inorganic phosphors and quantum dots, and to analyze prototype devices, despite their shortcomings. We then shift our analysis toward contemporary ideas in color theory that more accurately describe the color quality of modern LED light bulbs and flat-panel displays. Finally, the perspective examines the opportunities and challenges of applying these new concepts to guide the design of luminescent materials used in LED-based applications.

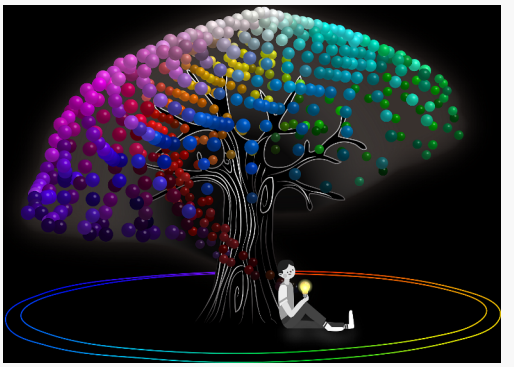

1. INTRODUCTION

The world was transformed approximately 150 years ago when the incandescent light bulb was improved to the point where artificial light could be reliably produced at a commercial scale. It was finally possible to begin replacing the sun, fire, or candles as our only sources to illuminate the world. From the earliest forms of electric lighting that used carbonized cotton and bamboo filaments to the improved tungsten-filament-based bulbs, incandescent lighting has made modern human civilization possible.[1] Indeed, artificial lighting has helped humans function equally during the day and at night, indoors and outdoors. The man-made source of this light was revolutionary, and yet incandescent lamps produce white light identical with the natural blackbody radiation—sunlight—that humans have been exposed to throughout our entire evolution. The only significant drawback of incandescent bulbs is that ≈95% of the electricity that they use is converted to heat, making these lights tremendously energy-inefficient.[2]

Today, lighting has moved beyond using blackbody radiation as our source of light to more energy-efficient light production. Modern methods use a semiconducting light-emitting diode (LED) combined with one or more inorganic phosphors. Unlike halogen and fluorescent light bulbs, whose line emissions were among the first alternative light sources that did not follow the blackbody curve, LED chips more efficiently convert electricity to a nearly monochromatic light that is used to excite the phosphor(s) coated on the chip's surface.[3] The resulting photoluminescence from the LED and phosphor blend creates a broadband emission spectrum that appears as white light to the human eye. The white light from these so-called phosphor-converted LEDs is functional and cheap to produce, but the emission spectrum is not continuous. Depressions appear in the white-light spectra stemming from the poor overlap between LED and phosphor emission or between the emission spectra of two phosphors. These areas, which are not present in a blackbody radiation curve, give some of these lights their notorious artificial appearance and imperfect color rendering in contrast to a blackbody radiator's natural appearance and perfect color rendering. Nevertheless, LED light bulbs are 75% more energy-efficient than incandescent or halogen bulbs, and they do not contain toxic mercury like fluorescent bulbs.[4,5] Phosphor-converted LEDs also have the advantage of being color-tunable. Changing the LED-to-phosphor emission intensity ratio or varying the phosphor blend are both approaches to tuning the light's color from a calming, warm white light to an energizing, cold white light.[6]

Fortunately, the crystal chemistry of inorganic phosphors is well understood, making novel phosphor design one of the most sought-after ways for tweaking phosphor-converted LED lighting. Phosphors are composed of a crystalline oxide, nitride, or halide host crystal structure substituted with a small

Received: September 23, 2021
Published: December 21, 2021

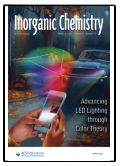

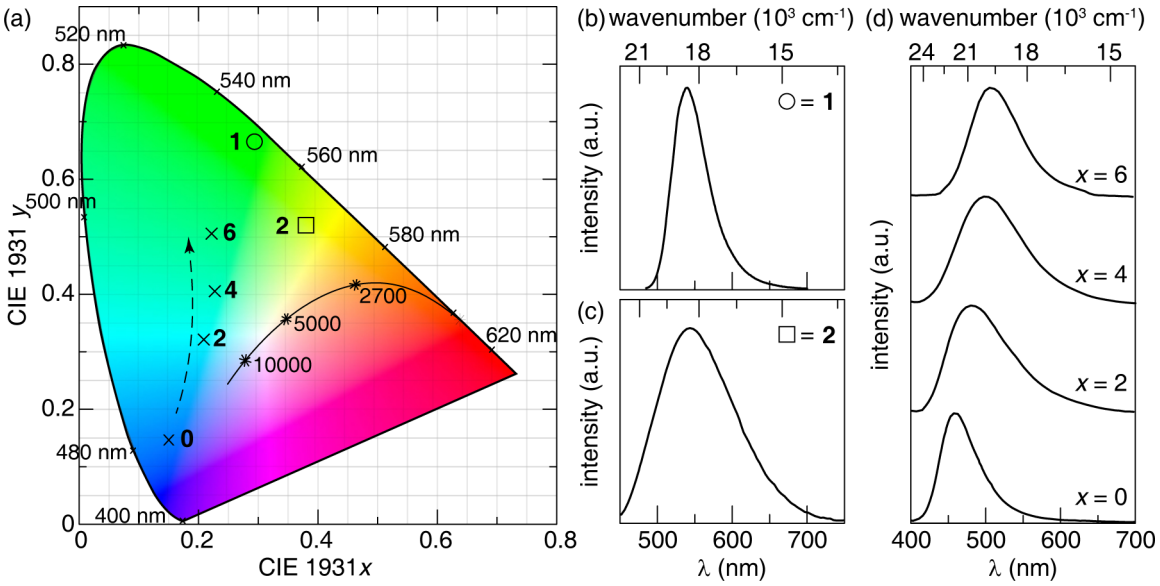

Figure 1. (a) 1931 CIE XYZ diagram representing all colors that the average human eye can perceive. Emission spectra of (b) β-SiAlON:Eu^{2+} (λ_{em} = 540 nm) where ○ = 1 (data were taken from ref 29) and (c) $Sr_{1.975}Ce_{0.025}Ba(AlO_4F)_{0.3}(SiO_5)_{0.7}$ (λ_{em} = 542 nm) where □ = 2 (data were taken from ref 31). The 1931 CIE XYZ coordinates of these phosphors are denoted as a circle and square in part a, respectively. (d) Emission spectra of $Ca_{2+x}La_{8-x}(SiO_4)_{6-x}(PO_4)_xO_2$:$Eu^{2+}$ (x = 0, 2, 4, and 6). The CIE coordinates are represented in part a by × (data were taken from ref 33).

percentage of a rare-earth or transition-metal activator ion. The composition and connectivity within the host crystal structure control the coordination environment and orbital energies of the activator, which determine the energy of the resulting optical transitions. In rare-earth-substituted phosphors, the magnitude of crystal-field splitting around the activator regulates the distance between the 4f and 5d orbitals that, in tandem with the nephelauxetic effect, control the photon absorption energy. Subsequent lattice relaxation guides the perceived color of the ensuing photon emission.[7] The choice of the host crystal structure also affects the efficiency and thermal stability of the phosphor emission. Decades of research have shown that crystalline hosts composed of dense bonding networks provide a rigid local structure that prevents the formation of nonradiative pathways, whereas wide optical band gaps help to prevent thermally induced photoionization.[8] The formalization of these design rules, among others, has allowed for new phosphor materials to be used in a myriad of advanced applications.

Phosphor-converted LED technologies were first applied in emergency signage and medical imaging and have slowly evolved to basic illumination.[9,10] Now, the development of high-powered LEDs and the discovery of efficient and thermally stable phosphors have allowed LED-based solid-state lighting devices to be used almost exclusively in modern domestic and commercial lighting, street lighting, car headlights, flat-panel LED televisions, monitors, laptops, tablets, and smartphones.[6,11−14] Given the diversity of uses for phosphor-converted LEDs, research on phosphors, in particular, has intensified dramatically to address many technological needs. The field has rapidly evolved from exploratory synthesis to creating computational methods, applying data science and machine learning, and building combinatorial chemistry tools to accelerate phosphor discovery.[15−19] The outcome is hundreds of new phosphor publications in peer-reviewed journals every month. Nevertheless, the optical properties and subsequent production of prototype phosphor-converted LED light bulbs or display panels, no matter how well described in these papers, often do not take human perception of light into account.

The underlying principles that dictate whether a novel luminescent material is appropriate for a specific application are based on color theory and how humans perceive light.[20] However, color theory is often overlooked or misapplied in the race to develop new phosphors and incorporate these materials in light bulbs, televisions, or monitors. The discussion here focuses on the experimental and theoretical studies that integrate colorimetry and the human perception of color in the development of new phosphor materials and creation of prototype solid-state LED-lighting devices. This Viewpoint first discusses the application and drawbacks of the original color theories often used in the literature today. We then expand to modern concepts in colorimetry that were developed in response to the rise of LED-based lighting. Finally, this Viewpoint suggests promising research directions that should aid the development of next-generation, high-color-quality LED-based white light.

2. CURRENT APPLICATIONS OF COLOR THEORY IN PHOSPHOR CHARACTERIZATION

2.1. Formulation of the 1931 CIE XYZ Color Space and Its Implications. Colorimetry is the field of science developed to quantify and describe the perception of color. Our brain's interpretation of color is a psychophysical response to photons in the visible region of the electromagnetic spectrum striking the retina. Light is detected at the back of the eye by photoreceptor rods and cones, which transmit signals to the optic nerve via retinal bipolar cells and ganglion neurons.[21,22] The latter are activated by the blue region of the visible spectrum to control humans' natural circadian rhythm.[23] Photoreceptors, on the other hand, are critical to human vision. Rods do not contribute to our color vision because they are equally sensitive at all wavelengths of light. Conversely, the combination of three unique cones, called short (420−440 nm), middle (530−540 nm), and long (560−

https://doi.org/10.1021/acs.inorgchem.1c02975
Inorg. Chem. 2022, 61, 4205−4218

580 nm), enables color vision.[24] The cones differ based on their peak spectral sensitivity in the blue, green, and red regions of the visible spectrum, respectively.[25] Different levels of stimuli affect the three types of cones independently, known as the tristimulus, which allows humans to perceive different colors.

The International Commission for Illumination (Commission Internationale de l'Eclairage, or CIE) was the first organization to standardize how the human eye perceives color. Their original creation was the 1931 CIE XYZ color space, which represents all colors visible to a person with average eyesight. This color space was formalized to serve as the first quantitative link between the distribution of wavelengths across the visible region of the electromagnetic spectrum and the physiology involved in the perception of color in human vision.[26] The CIE diagram was derived by determining spectral response curves that could mathematically describe humans' trichromatic vision. These color-matching functions, or the standard (colorimetric) observer, provided a standardized, numerical method to convert spectral radiance to trichromatic color space.[26,27] The resulting tristimulus values (X, Y, and Z) are converted to (x, y) coordinates to represent a specific color on the 1931 CIE XYZ color space.[25] The 1931 CIE XYZ diagram, illustrated in Figure 1a, is a two-dimensional mapping of the colors visible to the average human eye. The curved outer edge of the diagram, known as the spectrum locus, comprises monochromatic sources. The straight edge near the bottom is called the purple line, where the colors on this line are produced through the combination of blue and red sources.[28] All colors inside the spectrum locus directly result from the trichromatic nature of human perception, where the highly saturated colors lie near the locus and white falls near the center.

Mapping a perceptible color space is instrumental in conveying the emission color of luminescent materials like inorganic phosphors. For example, β-SiAlON:Eu^{2+} is arguably the most popular green-emitting phosphor used for display applications today owing to its narrow emission full width at half-maximum (fwhm) of 55 nm (1760 cm^{-1}), the impressive internal quantum efficiency of 97%, and thermally robust emission at 150 °C under blue-light excitation (λ_{ex} = 450 nm).[29,30] Applying the CIE's color-matching functions to analyze the emission spectrum of β-SiAlON:Eu^{2+} (Figure 1b) yields the 1931 CIE XYZ chromaticity coordinates that allow researchers to clearly illustrate this phosphor's brilliant green color, as shown within the circle plotted in Figure 1a. The superiority of β-SiAlON:Eu^{2+} can be further highlighted by comparing the emission from β-SiAlON:Eu^{2+} (λ_{em} = 540 nm) to another green-emitting phosphor, such as $Sr_{1.975}Ce_{0.025}Ba(AlO_4F)_{0.3}(SiO_5)_{0.7}$ (λ_{em} = 542 nm). Despite having an emission maximum nearly identical with β-SiAlON:Eu^{2+}, $Sr_{1.975}Ce_{0.025}Ba(AlO_4F)_{0.3}(SiO_5)_{0.7}$ has a significantly broader emission of 128 nm (4127 cm^{-1}), as shown in Figure 1c. The broadness of the emission hinders saturation of the green color, resulting in a more yellow-green hue, as shown within the square plotted in Figure 1a.[31] The 1931 CIE XYZ color space is an excellent way to display the relationship between the color saturation, emission maximum, and emission fwhm. Figure 1 also emphasizes the somewhat counterintuitive point that the perceived color is not just determined by the emission peak wavelength.[32]

The 1931 CIE XYZ color space is also used to easily visualize a phosphor's color tunability through chemical modification, such as the preparation of a solid solution. For example, the emission of $Ca_{2+x}La_{8-x}(SiO_4)_{6-x}(PO_4)_xO_2$:$Eu^{2+}$ (x = 0, 2, 4, and 6) red-shifts upon the incremental substitution of $[SiO_4]$ units for $[PO_4]$, as plotted in Figure 1d.[33] The actual shift in the perceived color is illustrated by plotting the 1931 CIE XYZ coordinates in Figure 1a as the × symbol. An obvious color change occurs from blue to green upon the incorporation of $[PO_4]$. This outcome is crucial because the 1931 CIE XYZ color space allows researchers to observe the exact range of colors produced by tailoring the composition of a phosphor.

The Planckian locus, which represents blackbody radiation at a specific temperature, is also usually included in the 1931 CIE XYZ color space. It is shown as the black solid line in Figure 1a. The locus goes from a deep red, indicating blackbody radiation at low temperatures (1500 K), to orange (2000 K), then to white (≈4000 K), and finally to bright blue (10000 K). The Planckian locus represents the actual temperature that a blackbody radiator must be heated to for a photon of that color to be emitted.[34] For example, incandescent light bulbs produce light through thermal radiation of a tungsten filament. The characteristic warm white light is produced when the bulb's filament reaches temperatures between 2000 and 3000 K while driving the filament above 5000 K produces a colder white light.[28] However, the light produced from nonblackbody sources, such as fluorescent and phosphor-converted LED light bulbs, does not arise from the same mechanism. Thus, a new scale, known as the correlated color temperature (CCT), was developed to describe the color of light from these sources. The CCT refers to the temperature required for a blackbody radiator to produce white light with chromaticity most similar to that of an artificial light source.[34] In this case, cold white fluorescent light bulbs with a CCT of 5000 K will generate white light similar to that of a blackbody radiator heated to ≈5000 K.[20,35]

Commercially available light bulbs are often marketed with their CCTs printed on the box to describe the hue of white light they produce. The simplest modern solid-state white light bulb design comprises a blue-emitting InGaN LED and a yellow-emitting phosphor, $Y_3Al_5O_{12}$:Ce^{3+}.[36] The phosphor absorbs the blue LED emission and partially downconverts the emission to produce yellow light, with the combination of blue and yellow emissions appearing as white light. The lack of an explicit red spectral component in these lights causes the resulting white light to appear cold and have a CCT between 4000 and 8000 K, depending on the ratio between the blue LED emission and yellow phosphor emission.[7] High CCT light (>5000 K) is not suitable for in-home or commercial lighting. Therefore, a second, highly efficient, thermally robust red-emitting phosphor such as $Sr_2Si_5N_8$:Eu^{2+} (λ_{em} = 618 nm; fwhm = 83 nm) or $CaAlSiN_3$:Eu^{2+} (λ_{em} = 650 nm; fwhm = 92 nm), among others, are included in the phosphor blend of commercial light bulbs.[37−39] Here, the ratio of blue, yellow, and red emissions controls the observed CCT. Solid-state lights that contain phosphor blends with a lower red spectral component relative to the blue LED emission are typically tuned to have a CCT of ≈5000 K. These lights are commonly used in offices and schools and are often referred to as "daylight" in commercially sold bulbs. These devices are indeed excellent for reproducing daylight indoors. In contrast, there is a strong preference for in-home lights to have a warmer white hue. This is made possible by increasing the contribution of red emission relative to the yellow phosphor and blue LED emissions.[40] The more intense red spectral component within

https://doi.org/10.1021/acs.inorgchem.1c02975
Inorg. Chem. 2022, 61, 4205−4218

the phosphor blend allows the CCT to be lowered and tuned to ≈2700 K to mimic the light created by a warm tungsten filament light bulb. These bulbs are often marketed as a "soft white" LED light bulb.

Interestingly, there are some instances where a single phosphor produces an ultrabroad emission that covers most of the visible spectrum, appearing as white light. $Sr_2AlSi_2O_6N:Eu^{2+}$ is one example of these unique compounds. This phosphor produces an emission centered at 600 nm with a fwhm of 230 nm (≈7057 cm^{-1}).[19] The broad emission stems from the presence of three crystallographically independent Sr^{2+} sites for rare-earth substitution. Combining this phosphor with an UV LED (λ_{em} = 375−380 nm) produces a white light with a CCT of ≈3900 K. It is clear through these analyses that the 1931 CIE XYZ diagram is the most straightforward method for visualizing the complex emission spectra of luminescent materials and reducing these data into a single (x, y) color point.

2.2. Maximizing the Color Gamut for Display Lighting. The 1931 CIE XYZ diagram is also widely employed in the development of materials for display lighting. The choice of red-, green-, and blue-emitting materials controls the range of colors produced by a screen or monitor. Connecting the CIE chromaticity coordinates of these three colors forms a triangle representing the palette of available colors, known as the color gamut. This is among the most defining visual characteristic of any display.[41] All image-based applications need a specific and well-defined color gamut to reproduce colors accurately, giving rise to many standard color gamuts. The first color gamut was established in 1953 by the National Television System Committee (NTSC) for color cathode-ray tube screens.[41] Cathode-ray tube screens produced colored images using three electron beams to excite a phosphor-coated screen of red-, green-, and blue-emitting materials. The phosphor emissions were then passed through a set of color filters, where the desired wavelength of light required to hit the gamut's color points was allowed to pass.[42] This caused most of the emission from a broadband phosphor to be filtered off, making these devices inherently inefficient. Narrow-emitting phosphors would have created a more efficient display by minimizing the amount of light that gets filtered out and by preventing light from leaking through the wrong color filter, such as broadband green emission through a blue filter.[43] Unfortunately, the ZnS-based phosphors utilized in the color television were broadband and not saturated enough to cover most of the NTSC-defined gamut (white triangle, Figure 2). In fact, the gamut produced by $ZnS:Ag^+$, $Zn_{1-x}Cd_xS:Cu^+$, and $Zn_{1-x}Cd_xS:Ag^+$ as the blue, green, and red emitters, respectively, led to only 60% of overlap with the NTSC gamut (gray dashed triangle, Figure 2).[44] The low NTSC coverage was further impacted from the desaturated yellow-green color point of $Zn_{1-x}Cd_xS:Cu^+$ stemming from its broad emission spectrum. Nevertheless, the ratio of Zn/Cd and the resulting color point were intentionally chosen to balance the ratio of the three primaries to create white light with higher luminance at the sacrifice of a narrower gamut.[44,45]

The poor performance of the ZnS-based materials spurred the search for new highly saturated blue-, green-, and red-emitting phosphors to maximize the overlap with the NTSC gamut. Because narrow-emitting phosphors tend to yield saturated 1931 CIE XYZ color coordinates, the phosphors utilized for display lighting must have a narrow emission (fwhm ≤ 40 nm) in addition to a high photoluminescent

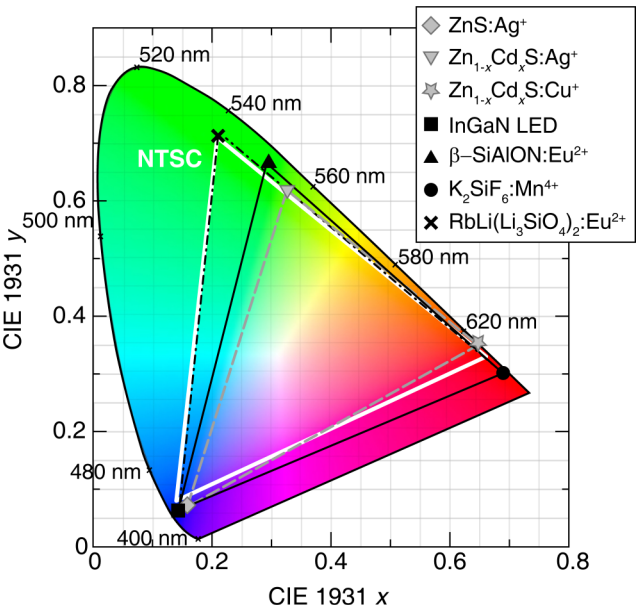

Figure 2. Color gamut (gray dashed line) produced by the first phosphors used in cathode-ray tube televisions: $ZnS:Ag^+$ (gray diamond), $Zn_{1-x}Cd_xS:Ag^+$ (gray upside-down triangle), and $Zn_{1-x}Cd_xS:Cu^+$ (gray star). Data were taken from ref 42. Wider color gamuts (black solid line) can be produced utilizing a blue-emitting InGaN LED (black square), β-$SiAlON:Eu^{2+}$ (black triangle), and $K_2SiF_6:Mn^{4+}$ (black circle). Data were taken from ref 30. Replacing β-$SiAlON:Eu^{2+}$ with green-emitting $RbLi(Li_3SiO_4)_2:Eu^{2+}$ (black ×) produces a color gamut (black dashed line) that covers nearly the entirety of the NTSC color gamut (white line). Data were taken from ref 48.

quantum yield and thermally robust emission.[46] This fundamental knowledge originally used for cathode-ray tube screens was eventually applied to the development of phosphor-driven flat-panel LED screens. Flat-panel LED screens contain a white LED backlight that produces white light by exciting a red and green phosphor blend with a blue LED. This white light also passes through color filters to split the light into individual red, green, and blue components that set the gamut.[43] The blue LED is ideal for display applications because its nearly monochromatic emission yields a highly saturated, deep-blue color. The CIE chromaticity coordinates of a blue LED (λ_{em} ≈ 450 nm; black square, Figure 2) lie just outside the vertex of the NTSC triangle, indicating excellent coverage of the blue region of the NTSC gamut. The blue LED not only is the blue color point but also functions as the excitation source for the red- and green-emitting phosphors. The most popular red-emitting inorganic phosphor used in today's displays is arguably $K_2SiF_6:Mn^{4+}$ because of its strong blue-light absorption and highly efficient, narrow line emission. The transition metal's electronic transition is spectrally equivalent to a Gaussian with a fwhm of 30 nm centered at 630 nm.[46] The 1931 CIE XYZ coordinates of $K_2SiF_6:Mn^{4+}$ (black circle, Figure 2) show that the red emission from this phosphor is more saturated than the red color point set by the NTSC, meaning that this material is better than the NTSC standard. Despite these excellent optical properties, this material has a relatively long luminescent lifetime of ≈8.8 ms, which can lead to adverse saturation effects and a lower absorption cross section compared to rare-earth-substituted materials. $K_2SiF_6:Mn^{4+}$ is also sensitive to moisture unless extra

https://doi.org/10.1021/acs.inorgchem.1c02975
Inorg. Chem. 2022, 61, 4205−4218

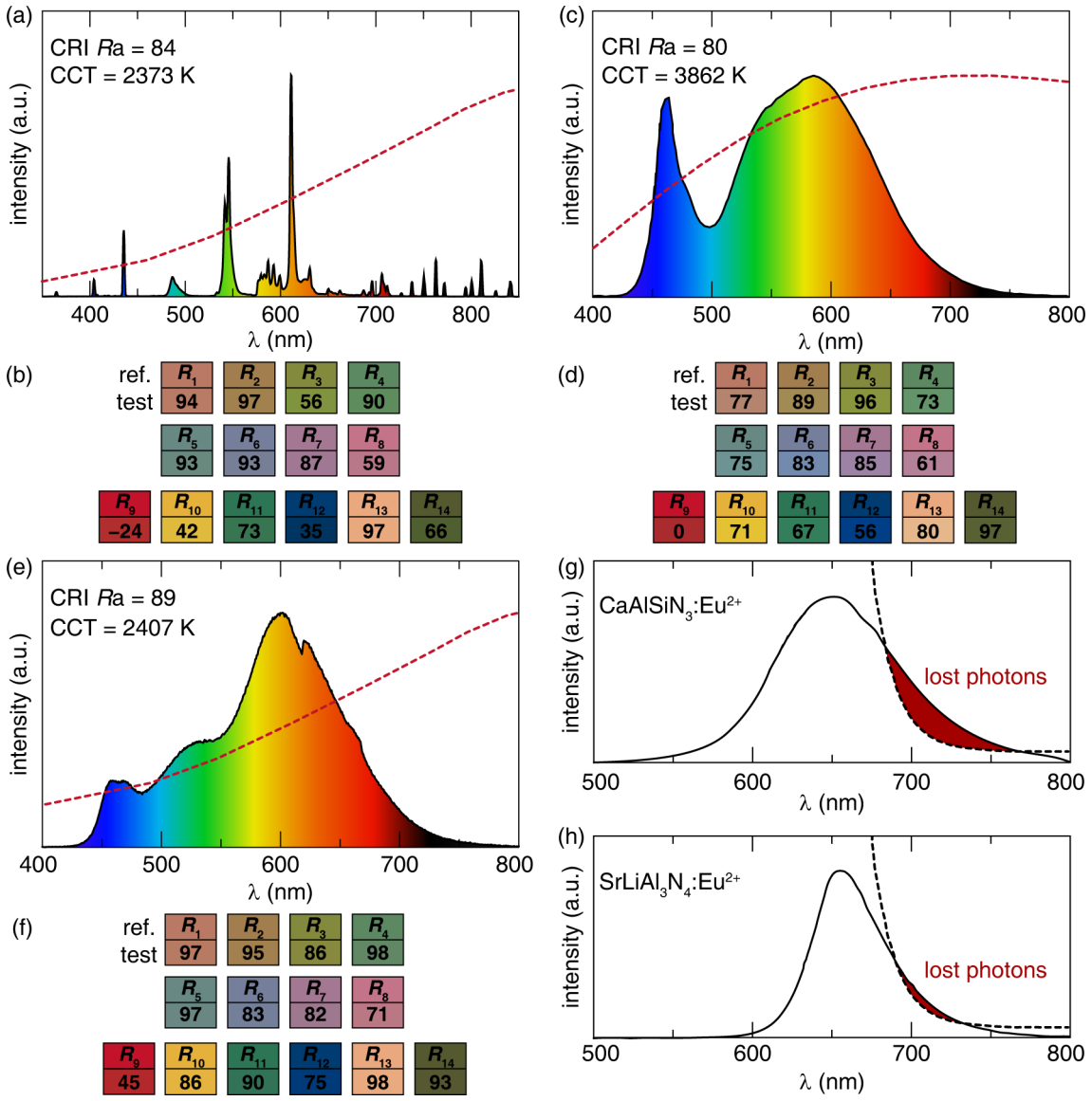

Figure 3. (a) White-light spectra produced by a compact fluorescent bulb and (b) the color of the Munsell samples when illuminated by a reference source (top) and the device (test, bottom). (c) Emission spectrum and (d) the color rendering from a device composed of an InGaN LED, $Y_3Al_5O_{12}:Ce^{3+}$, and $Sr_2Si_5N_8:Eu^{2+}$. Data were taken from ref 54. (e) Emission spectrum and (f) the color rendering of an InGaN LED, $NaBaB_9O_{15}:Eu^{2+}$, and $Sr_2Si_5N_8:Eu^{2+}$. Data were taken from ref 30. Blackbody radiation curves are provided as the red dashed line corresponding to the appropriate CCT. (g) Large portion of the emission spectrum of $CaAlSiN_3:Eu^{2+}$ lying outside the upper limit of the sensitivity of the average human eye (black dashed line) but (h) only a small portion of the emission from $SrLiAl_3N_4:Eu^{2+}$ lying outside the sensitivity limit of the average human eye. The overlap between the emission spectra and the limit of spectral sensitivity is highlighted in red. Data were taken from ref 40.

precautions are used.[46,47] The green-emitting phosphor of choice for display applications is β-SiAlON:Eu^{2+}, as previously mentioned, because it is one of the narrowest commercial green phosphors available today. Connecting the chromaticity coordinates of these three luminescent materials creates a gamut covering ≈72% of the NTSC (black solid triangle, Figure 2), which is a significant improvement over the ZnS-based phosphors.[30] It is obvious though that the green color point is still responsible for the less than complete NTSC coverage. Xia et al. recently reported a new green-emitting phosphor, $RbLi(Li_3SiO_4)_2:Eu^{2+}$, that potentially rivals β-SiAlON:Eu^{2+}.[48] This green-emitting phosphor has an emission band centered at 530 nm with a fwhm of 42 nm (1551 cm^{-1}) under blue-light (λ_{ex} = 460 nm) excitation. Plotting the 1931 CIE XYZ coordinates of $RbLi(Li_3SiO_4)2:Eu^{2+}$ (black ×, Figure 2) and creating a gamut with a blue LED and $K_2SiF_6:Mn^{4+}$ allows for a direct comparison of the gamuts created by $RbLi(Li_3SiO_4)_2:Eu^{2+}$ and β-SiAlON:Eu^{2+}. Interestingly, the gamut created by $RbLi(Li_3SiO_4)_2:Eu^{2+}$ shown as the dashed black line, covers 107% of the NTSC gamut because the 1931 CIE XYZ coordinates of this phosphor nearly overlap with that of the NTSC green color point.[48] It is evident through this analysis that using β-SiAlON:Eu^{2+} in our current displays does not allow access to the broadest color gamut possible, and further research should be done to maximize the color gamut coverage.

2.3. Evaluating Color Reproduction through the Color Rendering Index. Chromaticity does not provide all of the color information needed to describe a light source. Curiously, artificial light sources (i.e., nonblackbody radiators)

https://doi.org/10.1021/acs.inorgchem.1c02975
Inorg. Chem. 2022, 61, 4205−4218

do not necessarily reproduce the colors of an object accurately, whereas all blackbody radiation sources achieve perfect color reproduction. This property is referred to as color rendering. Color rendering is vital in color-critical settings such as museum lighting, restaurants, or retail stores. It has even proven critical in neonatal care units, where the appearance (color) of a newborn is often used to assess its health.[49]

The only internationally agreed-upon metric for evaluating color rendering is through the color rendering index (CRI). The CRI was first developed in 1971 to evaluate the color rendering performance of fluorescent lamps, the first commercialized nonblackbody artificial light source. The CRI is determined by calculating the 14 spectral CRIs, R_i, as the difference, ΔE_i, in the color rendering of a color sample between a reference source, typically a blackbody radiator because of its perfect color rendering, and the test light source using the 1964 CIE $U^*V^*W^*$ color space (eq 1).[20,25] The maximum value for R_i is 100, indicating no difference in color rendering between the reference and test light source. Negative values of R_i can be obtained if the color difference between the source and test is large.

$$R_i = 100 - 4.6\Delta E_i \quad (i = 1, \ldots, 14) \tag{1}$$

There are 14 standard test color samples, known as the Munsell samples, that the reference and test light source illuminate. The first eight Munsell samples are medium saturated colors and are evenly distributed across the visible region. The average R_i from the first eight Munsell samples yields the general CRI, R_a, which is generally used to relay the color rendering capabilities of a light source. The last six Munsell samples offer supporting information about the color rendering. Specifically, standard colors R_9−R_{12} represent the color rendering of highly saturated red, yellow, green, and blue, while R_{13} and R_{14} describe the color rendering of complexion and the color of leaves, respectively.

The CRI was first developed to evaluate the difference in color rendering between fluorescent bulbs and the perfect color rendering of incandescent bulbs.[35,50] Plotting the emission spectrum from a fluorescent bulb in Figure 3a shows that these lights have multiple discrete line emissions that in combination result in white light with a CCT of 2373 K. The spectrum also contains numerous regions, like from 500 to ∼530 nm, that barely cover the visible spectrum. By only covering certain wavelength regions of the visible spectrum, fluorescent bulbs cannot accurately reproduce every color in the visible spectrum, such as yellow-green, where R_3 is only 56 (Figure 3b). As a result, modern fluorescent bulbs have an overall CRI R_a of 80−87, which falls within the minimum required CRI R_a of 80.[51] This is distinct from a blackbody radiator whose broadband emission covers the entirety of the visible spectrum in a smooth, continuous manner (red dashed line, Figure 3), resulting in CRI R_a = 100.

The CRI is widely used by researchers today as the metric for evaluating the quality of light produced by all lamp types, including LED-based light bulbs, relative to a perfect blackbody source. A $R_a \geq 80$ is generally considered to be acceptable for indoor lighting, whereas a $R_a > 90$ is usually excellent. The simple LED "daylight" bulbs that combine the blue-emitting InGaN LED and yellow-emitting $Y_3Al_5O_{12}:Ce^{3+}$ typically have a R_a of only ≈70.[52] These devices have a prominent gap in the 480−520 nm region, known as the "cyan gap" and minimal red spectral coverage, reducing the CRI.[6,53] These absences are reflected in the spectral CRIs where the R_5 value, which represents light blue-green, is typically between 60 and 70, and the R_9 value representing highly saturated red is a negative value, such as −44. The R_9 value is readily improved by adding a red phosphor like $Sr_2Si_5N_8:Eu^{2+}$ to produce a warmer white light (CCT = 3862 K).[54] Recalculating the CRI utilizing InGaN, $Y_3Al_5O_{12}:Ce^{3+}$, and $Sr_2Si_5N_8:Eu^{2+}$ yields an improved R_9 of 0 because of better coverage of the 620−700 nm region (Figure 3c). It is essential to note that this R_9 value still indicates poor rendering of highly saturated red. Nevertheless, adding a red-emitting phosphor is the only approach to improve the R_a to 80 because the slight increase in the red region improves the medium saturated color rendering (R_5 = 75, Figure 3d).[54−56] For this reason, "soft white" LED light bulbs composed of InGaN, $Y_3Al_5O_{12}:Ce^{3+}$, and a red-emitting phosphor have been commercially produced at low cost for consumers.

The R_a can be most easily improved by adding additional phosphors or utilizing broadband-emitting phosphors in a device to cover most of the visible spectrum. This strategy is based on mimicking the spectra of blackbody radiators, which have perfect color rendering. In addition, this allows issues like the cyan gap to be resolved. The cyan gap in "soft white" LED light bulbs appears because of the minimal overlap between the emission spectra of the nearly monochromatic InGaN LED and the phosphors. The color rendering can be improved by using phosphors with an appropriate emission peak position and a fwhm broad enough to fill the cyan gap. For example, the emission spectrum of β-SiAlON:Eu^{2+} is typically too narrow to cover the cyan gap. The most popular broadband green-emitting phosphor for solid-state lighting is $Lu_3Al_5O_{12}:Ce^{3+}$ ($\lambda_{em} \approx 550$ nm) because of its high efficiency and excellent blue-light absorption.[57] As a result, many prototypes and commercial light bulbs use $Lu_3Al_5O_{12}:Ce^{3+}$ and a red-emitting phosphor to downconvert blue LED emission and produce white light. Unfortunately, even though the fwhm of $Lu_3Al_5O_{12}:Ce^{3+}$ is quite broad (fwhm = 103 nm, 3474 cm^{-1}), there is still a cyan gap in the white-light spectrum because of the position of the emission maximum.[58] Alternatively, it is possible to use the $NaBaB_9O_{15}:Eu^{2+}$ phosphor, which has a deep-green emission (λ_{em} = 515 nm) and a fwhm of 61 nm (2294 cm^{-1}).[30] Combining this material with red-emitting $Sr_2Si_5N_8:Eu^{2+}$ and a blue LED produces an impressive R_a of 89 (Figure 3e). The device has superior color rendering capabilities based on the values of R_1−R_8, which all exceed 70, shown in Figure 3f, as a direct result of using this green-emitting phosphor. $NaBaB_9O_{15}:Eu^{2+}$ specifically provides excellent color rendering of saturated green (R_{11} = 90) while covering the cyan region of the visible spectrum, yielding an impressive R_5 of 97 for blue-green rendering (Figure 3f).

2.4. Determining the Appropriate Balance between Color Rendering and Energy Efficiency. The spectrum produced by a white-light source affects not only the color rendering but also the energy efficiency of the light.[55] The energy efficiency is evaluated by determining the luminous efficacy of a light, a term used to describe the conversion efficiency from the input, electrical power (watts), to the output, luminous flux (lumens). The luminous efficacy of a light source is dependent on two factors: the conversion efficiency from electrical power to optical power, called the radiant efficiency (unweighted), and the conversion from optical power to luminous flux, which is the lumen output weighted against the sensitivity of the average human eye to the visible region.[20] The latter conversion is known as the

https://doi.org/10.1021/acs.inorgchem.1c02975
Inorg. Chem. 2022, 61, 4205−4218

luminous efficacy of radiation (LER), which has a theoretical maximum of 683 lm/W from a monochromatic 555 nm light source. This wavelength corresponds to the green region of the visible spectrum and is where the human eye has the highest spectral sensitivity.[28]

There is an inherent trade-off between the luminous efficacy and color rendering. Maximizing the luminous efficacy requires a nearly monochromatic source, whereas color rendering is best achieved using a broadband spectrum distributed evenly across the visible spectrum.[59] This phenomenon is most clearly observed by varying the ratio of yellow-emitting $Y_3Al_5O_{12}:Ce^{3+}$ and red-emitting $CaAlSiN_3:Eu^{2+}$ (λ_{em} = 650 nm; fwhm = 92 nm) in prototype devices and monitoring the simultaneous change in R_a and luminous efficacy.[60] Table 1 shows that the spectrum produced from 1 wt % $CaAlSiN_3:Eu^{2+}$ and $Y_3Al_5O_{12}:Ce^{3+}$ has a moderate efficiency of 122 lm/W but poor color rendering (R_a = 58). Incrementally increasing the amount of $CaAlSiN_3:Eu^{2+}$ in the phosphor mixture improves the R_a, reaching a maximum of 76.1 at 5 wt % $CaAlSiN_3:Eu^{2+}$. The consequence of enhancing the color rendering is a 70% decrease in this device's overall efficiency to 37 lm/W.

Table 1. Color Properties and Efficiency of Devices Containing $Y_3Al_5O_{12}:Ce^{3+}$ and Varying Weight Percentages of $CaAlSiN_3:Eu^{2+}$ (Reproduced with Permission from Reference 60. Copyright 2004 American Ceramic Society)

wt % $CaAlSiN_3:Eu^{2+}$	luminous efficacy (lm/W)	CCT (K)	CRI R_a	1931 CIE x	1931 CIE y
1	122	3539	58	0.448	0.511
2	131	3000	66	0.451	0.469
3	57.3	2886	68.6	0.431	0.379
4	45	2508	69.6	0.430	0.347
5	37	3777	76.1	0.346	0.242

The main reason for such a dramatic loss of efficiency is that a portion of the $CaAlSiN_3:Eu^{2+}$ phosphor's red emission falls outside the upper limit of sensitivity of the average human eye, shown as the black dashed line in Figure 3g. Photons emitted above this line penalize the LER because of the inherent inefficiency in producing light that humans cannot see.[40,56] This also contributes to the inefficiency of fluorescent light bulbs; the discrete optical transitions located in the imperceptible near-UV and near-IR regions of the electromagnetic spectrum plotted in Figure 3a penalize the LER.[28] These examples demonstrate the trade-off between the color rendering and LER. Despite this fundamental relationship, careful tuning of the emission spectra can allow trichromatic sources to achieve good color rendering and high luminous efficiencies.[36] The efficiency of LED-based light bulbs can be maximized by the development of red-emitting phosphors with emission bands located entirely within the spectral sensitivity region of the average human eye. One such promising phosphor is $SrLiAl_3N_4:Eu^{2+}$. This material produces a bright-red emission band centered at 655 nm with a fwhm of 52 nm.[40] As plotted in Figure 3h, only a small fraction of the emission band, highlighted in red to represent the lost photons, extends beyond the upper limit of human sensitivity. Therefore, $SrLiAl_3N_4:Eu^{2+}$ can potentially increase the CRI of a device while minimizing efficiency loss.[40] Similarly, Mn^{4+}-substituted fluorides, like $K_2SiF_6:Mn^{4+}$, have narrow line emissions, which limit the amount of photons lost into the near-IR.[61,62] The intense red line emission is spectrally equivalent to a Gaussian centered at 630 nm with a fwhm of 30 nm, which meets the spectral requirements for high-color-quality lighting.[63] As a result, General Electric uses this phosphor in their TriGain luminaires to simultaneously reduce the CCT and improve the CRI while maintaining the LER.[46]

An alternative route to maximizing the optical properties and efficiency includes utilizing a violet LED ($\lambda_{em} \approx 405$ nm) and blue-, green-, and red-emitting phosphors. Phosphor-converted light bulbs can use violet LEDs to cover the 400−450 nm range, which is lost when utilizing a blue LED. For example, the white-light spectrum from a mixture of blue-emitting $Na_2MgPO_4F:Eu^{2+}$, β-SiAlON:Eu^{2+}, and $Sr_2Si_5N_8:Eu^{2+}$ driven by a violet LED covers the entirety of the visible region while staying nearly within the limits of human perception. The prototype device has an impressive CRI R_a of 93 and an LER of 279 lm/W, which is comparable to the LER of a commercial bulb that is driven by a blue LED (LER = 359 lm/W) with a lower CRI R_a = 83.[64] This indicates that next-generation solid-state lighting devices should be designed to maximize overlap with the range of spectral sensitivity of the average human eye to more evenly balance the improvement of the color rendering and energy efficiency in LED light bulbs.

3. MODERNIZING LIGHTING EVALUATION WITH LEDS IN MIND

The 1931 CIE XYZ color space (1931), NTSC gamut (1953), and CRI (1965) were each developed to evaluate the quality of light produced by cathode-ray tube screens and fluorescent lamps and are still being applied today in the characterization of new phosphor materials and prototype devices.[41,65] These metrics, however, were developed before the invention of the high-brightness blue LED in 1993. Unfortunately, most of these metrics do not account for the superior optical properties provided by new LED-based devices. The rapid commercialization of LED-driven devices in general illumination and display technology has revealed many shortcomings in the original color-quality metrics. The following section discusses the limitations of these color-quality evaluation tools and suggests ways to apply modern color theory principles to improve the design of next-generation LED lighting and display technologies.

3.1. Evaluating Chromaticity Differences through the 1976 CIE *L*u*v (CIELUV).** The 1931 CIE XYZ color space was the first quantitative method to translate emission spectra into a perceived color and allowed for easy color discrimination and specification. Nevertheless, the 1931 CIE XYZ color space is not perceptually uniform, meaning a numerical change in the CIE coordinates does not correspond to a similar magnitude of perceived color change.[65] For this reason, the 1931 CIE XYZ color space is not adequate for evaluating chromaticity differences. Instead, the CIE developed the nearly uniform 1976 CIELUV color space for calculating chromaticity differences. The CIELUV coordinates are obtained by applying a nonlinear function on the X, Y, and Z tristimulus values to form a nearly uniform color space.[65] In the CIELUV, L^* represents perceptual lightness, i.e., light versus dark, ranging from 0 (black) to 100 (white). The tristimulus yields values of u^*, and v^* values are used to calculate the chromaticity coordinates (u', v') that are plotted on the 1976 CIELUV diagram.

The 1976 CIELUV is particularly useful for interpreting color shifts in a phosphor or light bulb during operation. LED-based devices typically generate heat during operation, where

https://doi.org/10.1021/acs.inorgchem.1c02975
Inorg. Chem. 2022, 61, 4205−4218

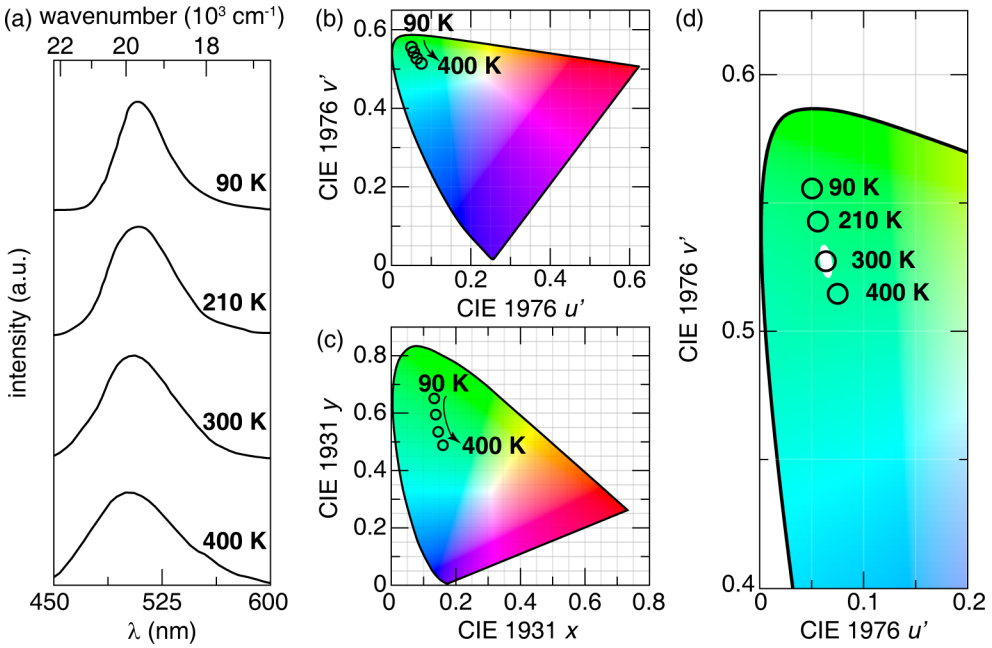

Figure 4. (a) Temperature-dependent emission spectra of Ba_2SiO_4:Eu^{2+}. The chromaticity coordinates of Ba_2SiO_4:Eu^{2+} are plotted on the (b) 1976 CIELUV and (c) 1931 CIE XYZ color spaces. (d) Three-step MacAdam ellipse (white) centered on the 300 K 1976 CIE chromaticity coordinates revealing the chromatic instability of Ba_2SiO_4:Eu^{2+}. Data were taken from ref 66.

the device can reach temperatures up to ≈400 K. The high temperatures have been known to affect a phosphor's emission peak shape, intensity, and position.[7] The uniform CIELUV color space correlates a phosphor's changing emission spectrum as a function of the temperature and the resulting differences in the perceived color of the phosphor in terms of the distance between the (u', v') chromaticity coordinates. For example, Ba_2SiO_4:Eu^{2+} is a well-known phosphor because of its bright-green emission. Running this phosphor at elevated temperatures causes some changes to the optical properties, such as a decrease in the photoluminescence intensity and a broader emission peak, as plotted in Figure 4a.[66] The 1976 CIELUV chromaticity coordinates, provided in Figure 4b, illustrate the slight shift in the phosphor's emission color away from the highly saturated green region, resulting from the emission spectrum broadening as a function of increasing temperature. Regardless, the position of the emission band is relatively unaffected, so the temperature-dependent chromaticity coordinates overlap. This suggests that the emission from Ba_2SiO_4:Eu^{2+}, as seen from the average human eye, should have only a slight change in the perceived color at high temperatures. Plotting the chromaticity coordinates of these emission spectra on a 1931 CIE XYZ color space (Figure 4c) shows a significant shift in the chromaticity coordinates. The original 1931 color space is misleading because it portrays a considerable difference in the perceived color because the distance between the chromatic coordinates is large. This is a direct result of the nonuniformity of the color space. The 1931 CIE XYZ color space clearly penalizes this phosphor for what is only a slight shift in perceived color. Thus, researchers should use the CIELUV color space for a more reliable description of perceived chromaticity differences as a function of the distance between two sets of chromaticity coordinates, especially when considering the effects of applied stimuli like temperature or applied current or when demonstrating how color shifts when the chemical composition is changed in a solid solution.

3.2. Classifying Perceptible Color Differences Using MacAdam Ellipses. Creating the uniform CIELUV color space has allowed researchers to address how a material's chromaticity coordinates and perceived color evolve. However, the CIELUV does not indicate whether the shift in chromaticity is distinguishable by the average human eye. Distinguishable chromaticity differences need to be specified to account for any changes in perceived color during a device's operational lifetime. The creation of the MacAdam ellipses met this need. David MacAdam was assigned by the photography company Kodak Inc. to determine how accurately the human eye could differentiate between similar colors. Through color-matching experiments involving human test subjects, MacAdam noticed that the color matches determined by the human subjects were not perfect matches, but all of the "match" colors fell within an ellipse that could be plotted on the CIE color spaces. These ellipses, now known as MacAdam ellipses, vary in size and orientation, but each encloses a series of colors indistinguishable to the human eye.[67] The ellipses are described using numerical steps representing the same number of standard deviations away from the reference color point. The creation of the MacAdam ellipses is instrumental to lighting because it allows researchers to express a tolerance around a target color.[68] Lighting companies, for example, typically require their materials to fall within a three or four-step MacAdam ellipse during their operational lifetime. Conversely, two devices made with two different phosphor blends should have chromaticity coordinates within a two-step MacAdam ellipse to ensure that comparisons of the color rendering or LER are being made for light sources with indistinguishable perceived colors.[69]

Employing MacAdam ellipses as a standard consideration in LED lighting design is crucial because it allows researchers to determine when a color shift causes a meaningful difference in

https://doi.org/10.1021/acs.inorgchem.1c02975
Inorg. Chem. 2022, 61, 4205−4218

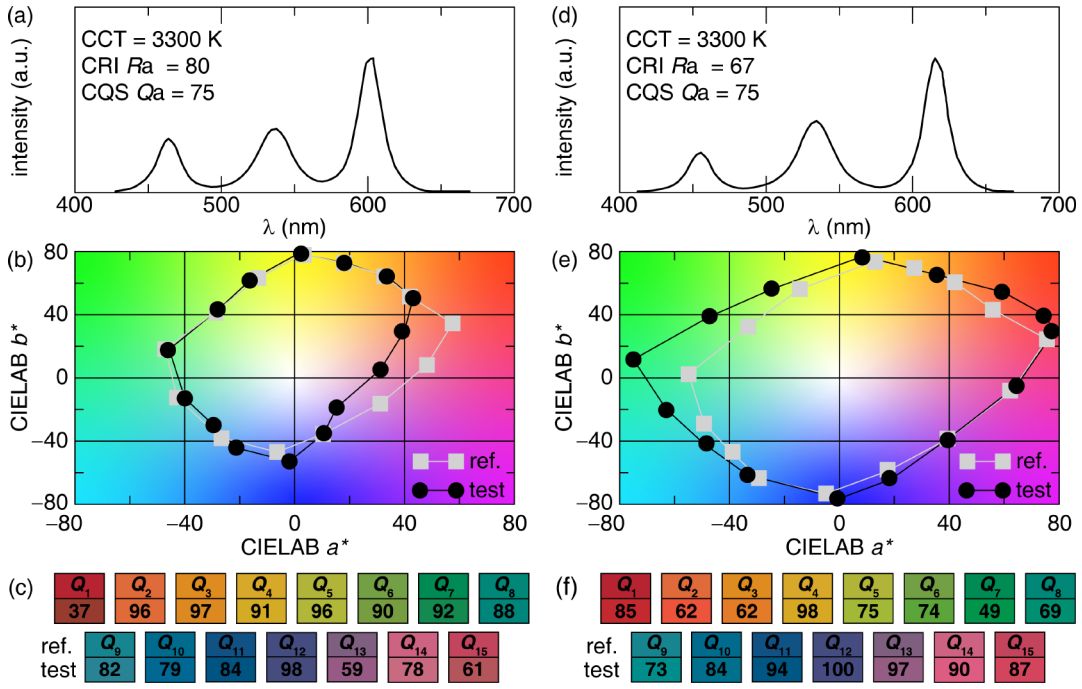

Figure 5. (a) Simulated white-light spectrum from blue, green, and red LED emissions centered at 466, 538, and 603 nm, respectively. (b) CIELAB chromaticity coordinates of 15 saturated color objects and (c) the color of the 15 Munsell samples when illuminated by a reference source (gray squares, ref.) and the simulated spectrum (black circles, test) in (part a. (d) Simulated white-light spectrum from blue, green, and red LED emissions centered at 455, 534, and 616 nm, respectively. (e) CIELAB chromaticity coordinates of 15 saturated color objects and (f) the color of the 15 Munsell samples when illuminated by a reference source (gray squares, ref.) and the simulated spectrum (black circles, test) in part d. Adapted with permission from ref 50. Copyright 2010 Society of Photo-Optical Instrumentation Engineers.

the color perceived by the average human eye. The temperature-dependent chromaticity shifts of $Ba_2SiO_4:Eu^{2+}$ can now be qualified based on this analysis. A three-step MacAdam ellipse centered on the room temperature (300 K) chromaticity coordinates reveals that at 400 K, the operational temperature of many LED-based devices, the perceived emission color is distinguishable from the room temperature color (Figure 4d). Thus, the perceived color of any light that uses this phosphor would be noticeably different as the bulb's operational temperature increases. In contrast, the green emission color from $NaBaB_9O_{15}:Eu^{2+}$ appears invariant to the average human eye from 300 to 680 K because the high-temperature chromaticity coordinates lie within the room temperature three-step MacAdam ellipse.[30] This indicates that $NaBaB_9O_{15}:Eu^{2+}$ is more chromatically stable than $Ba_2SiO_4:Eu^{2+}$. This analysis is essential and should be applied to interpret the emission color of all new luminescent materials and their prototypes to support claims of "chromatic stability" and avoid noticeable color drifts in light sources and displays.

3.3. Transitioning to the Color-Quality Scale Using the 1976 CIE *L*a*b (CIELAB) Color Space.** While the 1976 CIELUV color space and MacAdam ellipses are used to evaluate chromaticity differences, these scales are not involved in determining the color rendering. The first color space the CIE developed to calculate the color rendering was the nearly uniform 1964 CIE $U^*V^*W^*$ color space. This color space is outdated and no longer recommended to evaluate color differences.[65] For this reason, in 1976, the CIE concurrently developed an improved nearly uniform color space, the 1976 CIELAB, to calculate color rendering differences. This color space is described by L^*, which represents perceptual lightness, while a^* and b^* represent the ratio between the contrasting colors, red-green and yellow-blue, respectively.[70] This three-dimensional color space measures color differences as the Euclidean distance between two sets of color chromaticity coordinates (a^*, b^*).[71] Perfect color rendering occurs when the chromaticity coordinates of a test light source overlap entirely with the coordinates of a blackbody reference.

It is surprising that the CRI, the scale most commonly used to evaluate color differences, is still based on the obsolete 1964 CIE $U^*V^*W^*$ color space.[50] This is just the first of many shortcomings of the CRI. The CRI measures the color reproducibility of 14 Munsell samples, yet the equation used to calculate the value of R_i (i = 1, ..., 14) given in eq 1 only specifies the upper bound of R_i as 100 for perfect color rendering, leaving the lower boundary unrestricted. This makes it difficult to compare the color rendering abilities of two light sources, such as a cool white fluorescent lamp with an R_9 value of −89 versus a high-pressure sodium lamp with an R_9 value of −214.[20] The color rendering of saturated red is virtually nonexistent in both devices, and the different negative R_9 values do not convey any real variation in the rendering. Moreover, R_a is determined through the mathematical average of R_1−R_8. Averaging allows a light source to have a comparatively high R_a even if the light renders one or two colors poorly. Most importantly, the eight Munsell samples used to determine R_a are of low chromatic saturation. This means that a light source is not penalized for the poor color rendering of highly saturated colors, which is especially problematic considering that the current energy-efficient light bulbs and monitors are driven by nearly monochromatic and highly saturated LEDs.

The inability to directly compare the color rendering of light sources, along with the rapid commercialization of LED-based

https://doi.org/10.1021/acs.inorgchem.1c02975
Inorg. Chem. 2022, 61, 4205−4218

lighting, motivated researchers at the National Institute of Standards and Technology to develop the color-quality scale (CQS) in 2010. The CQS uses the 1976 CIELAB color space to determine the color rendering differences of 15 highly saturated color samples by a test and references light source. Saturated color samples were chosen because computational models have shown that a light source that reproduces saturated colors well would never poorly render desaturated colors.[50] After the difference in color reproduction is determined, a saturation factor is applied. This factor negates any contributions to color differences that arise from improved color saturation, meaning the source is neither rewarded nor penalized for increased saturation. The resulting values are the special CQS, or Q_i (i = 1, ..., 15). The calculation of the general CQS, Q_a, addresses the concerns of the CRI R_a by using the root mean square of all 15 color differences to equally weigh the color reproducibility of each color sample and applying a scaling factor so the CQS Q_a falls within 0 to 100. For a more in-depth review on the development of the CQS, the reader is directed to Ohno's *Color Quality Scale*.[50]

The advantages of the CQS and the limitations of the CRI are demonstrated using two hypothetical white-light LED simulations. The first simulated white-light spectrum is composed of blue, green, and red LED emissions centered at 466, 538, and 603 nm, respectively (Figure 5a). This light source has a CCT of 3300 K and a R_a of 80, indicating that the color rendering of this device is just acceptable for indoor lighting. Interestingly, while R_a suggests that this source may be utilized, the R_9 value of this device is −110, illustrating how R_a can be misleading because it is derived from the average of R_1−R_8 and does not consider the rendering of highly saturated colors. The 1976 CIELAB coordinates of the 15 saturated color objects (not to be confused with the Munsell samples) when illuminated by a reference and the simulated source significantly deviate in the saturated red and purple regions of the color space (Figure 5b). This indicates that this device would poorly render these colors, which is also reflected in the rendering of the Munsell samples seen in Figure 5c. This test source is appropriately penalized for this using the CQS; the Q_a value of this simulated light source is only 75, which would prevent this device from being used for indoor lighting.

A second simulated spectrum with blue, green, and red LED emissions centered at 455, 534, and 616 nm, respectively, plotted in Figure 5d, has an identical CCT of 3300 K but a R_a value of only 67. The CIELAB plot in Figure 5e shows that the CRI unfairly penalizes the light source for deviating from the reference source by having a more saturated color point in the green region. The difference, in reality, increases the color gamut and produces light that appears more appealing to the average human.[50] However, the CQS does not reward increased saturation, meaning that Q_a is identical with that of the first LED spectrum. It is important to note that this does not indicate that these two light sources reproduce color equally. The simulation depicted in Figure 5a is penalized for poor saturation of red (Q_1 = 37), purple (Q_{13} = 59), and pink (Q_{15} = 61), whereas the simulation in Figure 5d is penalized for the poor rendering of the large color difference between the saturated green colors (Q_6 = 74; Q_7 = 49; Q_8 = 69; Figure 5f), regardless of this source rendering these color samples with increased saturation. The CQS exposes the current generation of LED light bulbs that cannot render highly saturated colors well. Therefore, one possible future direction in the development of solid-state lighting devices is determining the appropriate combination of phosphors that yields an excellent rendering of saturated colors. It is conceivable that simulations of white-light spectra can also be used to create high-color-rendering light sources. Simulated white-light spectra that maximize Q_a can be modeled to guide the choice of phosphors depending on the fwhm, position, and shape of the emission bands used in the simulation. The derivation for the white LED simulation program can be found in *Spectral Design Considerations for White LED Color Rendering*.[20]

3.4. Analyzing Display Materials with the Rec. 2020 Color Gamut. The invention of the modern blue LED chip transformed display technology and spurred the search for new highly saturated phosphors that maximize the color gamut. Most display phosphors published today are being evaluated using the 1953 NTSC color gamut. While this was the first official standard color gamut, the primary color points chosen in the NTSC were too saturated and unattainable using the luminescent materials available in the 1950s. As a result, the NTSC was never considered to be an actual standard color gamut and is not used in any consumer content.[41] This begs the question of why, more than 70 years later, phosphors are still being analyzed using the obsolete NTSC gamut when the potential of new materials is discussed in publications. The phosphors that were used in early color televisions actually established the SMPTE-C color gamut (1968).[72] Since then, many additional and attainable color gamuts have been developed, such as sRGB/Rec. 709 (1993), Adobe RGB (1998), and DCI-P3 (2008) color gamuts.[72,73] Most of these gamuts are used in commercial devices such as 4K UHD televisions and high-end digital cameras.[41] The next-generation color gamut is the notably large ITU-R color space recommendation BT. 2020 standard color gamut, commonly referred to as the Rec. 2020 gamut (2012). The Rec. 2020 is 72% larger than sRGB/Rec.709 and 37% larger than DCI-P3, allowing the reproduction of colors beyond even the most recent gamuts.[41]

The Rec. 2020 color gamut is plotted as the white solid line on the 1931 CIE XYZ color space in Figure 6. The primaries of this gamut are all extremely saturated, such that few existing displays come close to providing the full range of colors specified. It may be possible to use an InGaN LED, $RbLi(Li_3SiO_4)_2:Eu^{2+}$, and $K_2SiF_6:Eu^{2+}$ to cover 107% of the NTSC color gamut, as described above, but the calculated overlap area when using these same primaries is only 76% of the Rec. 2020 gamut (gray dashed line, Figure 6). Thus, the overlap area must be improved by developing new saturated red-, green-, and blue-emitting luminescent materials. One such promising material is green-emitting γ-AlON:Mn^{2+},Mg^{2+}. The color gamut formed by using this green emitter with a blue LED and red-emitting $K_2SiF_6:Eu^{2+}$ improves the Rec. 2020 color gamut to 78% coverage.[74] More drastic improvements in the fulfillment of the Rec. 2020 have been reported by using $K_2GeF_6:Mn^{4+}$, an isostructural derivative of $K_2SiF_6:Mn^{4+}$.[75] The calculated color gamut from $K_2GeF_6:Mn^{4+}$, γ-AlON:Mn^{2+}, Mg^{2+}, and a blue LED covers 85% of the Rec. 2020, seen as the gray solid line in Figure 6.

These materials are some of the few examples of phosphors that approach fulfillment of the Rec. 2020 gamut, indicating that there is still a need for highly saturated phosphors to satisfy the entirety of this standard gamut. One potential avenue in the rapid discovery of new luminescent materials is through the single-particle diagnosis approach, where phosphors from polycrystalline samples that exhibit appropri-

https://doi.org/10.1021/acs.inorgchem.1c02975
Inorg. Chem. 2022, 61, 4205−4218

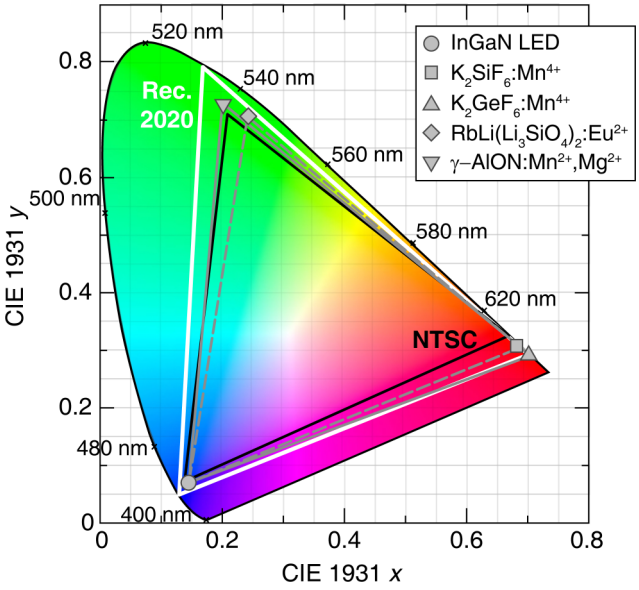

Figure 6. Color gamut produced by an InGaN LED (circle), $K_2SiF_6:Mn^{4+}$ (square), and $RbLi(Li_3SiO_4)_2:Eu^{2+}$ (diamond), indicated by the gray dashed line, having an overlap area of 76% with the Rec. 2020 standard color gamut (white) when plotted on the 1931 CIE XYZ color space. Data were taken from ref 48. The overlap area can be improved to 85% by using an InGaN LED, $K_2GeF_6:Mn^{4+}$ (up-triangle), and γ-AlON:Mn^{2+},Mg^{2+} (down-triangle). Data were taken from ref 74. The NTSC color gamut (black) is provided for reference.

ately narrow and bright emission under blue-light excitation can be selected from a bulk sample for crystal structure analysis.[76] The optimal materials can then be scaled up for production. Derivatives of new materials can also be developed through solid solutions or structural modification.[31,37,77,78] Alternatively, with publications on phosphors coming out daily, data sets containing the absorption, emission, substitution site symmetry, and other properties of phosphors can be constructed and used to train machine-learning models to rapidly identify new ultranarrow-emitting phosphors.[17,79,80] Researchers have also shifted their focus to using quantum dots to cover the red and green regions of the Rec. 2020.[41] The chemical stability and toxicity of these materials hindered their initial widespread use in display technology. However, QLEDs have started to make their way to the marketplace.[25] In addition, the current generation of blue LEDs have outstanding optical properties, including a fwhm of ≈25 nm. Yet, it is obvious from Figure 6 that the LED emission and the resulting chromaticity coordinates are not yet saturated enough to reach the vertex of the Rec. 2020, which represents the deep-blue color required to fulfill the gamut.[81] The discovery of blue-emitting organic-light-emitting-diode materials may provide the ultimate solution for display applications, providing the necessary high efficiencies, narrow emission bands, and physical flexibility that could transform future display lighting.[82]

4. CONCLUSION AND OUTLOOK

This Viewpoint presents a brief overview of the current applications of color theory in the characterization of phosphor materials and solid-state lighting devices. Phosphors reported today are often characterized using the CRI and NTSC color gamut, which provide an outdated and sometimes misleading characterization of the color quality of new phosphors and prototype devices. The spectral design of next-generation luminescent materials and solid-state lighting devices must consider modern colorimetric characterization techniques developed in response to the rise of LED-driven technology. The use of each metric is dependent on the potential application of the material. At a minimum, researchers should utilize the 1976 CIELUV color space when discussing the evolution of chromaticity coordinates as a function of the applied stimuli, McAdam ellipses to determine chromatic stability, and the CQS to evaluate color rendering. The Rec. 2020 gamut is specifically helpful for determining the suitability of a material for display lighting. Each of these metrics provides invaluable guidance for interpreting the properties of advanced materials.

This transition to high-quality lighting and display devices starts with the intentional use of these modern colorimetrics to highlight the areas in which our current solid-state lighting devices are lacking. This transition should not be difficult considering that commercial software such as PTI FelixGX (Horiba), fluorEssence (Horiba), Fluoracle (Edinburgh Instruments), and AvaSoft8 (Avantes), among others, is capable of generating many of these data, including mapping of the different color spaces and determination of the chromaticity coordinates. Alternatively, researchers can download the open-source program *ColorCalculator* directly from the OSRAM Web site; it can execute much of the advanced colorimetric analysis highlighted in this work, including calculating MacAdam ellipses and evaluating color rendering through the CQS.

The next generation of high-color-quality lighting and display devices can only be achieved by meeting the requirements set forth by advanced colorimetric analysis. These metrics have been known for decades, yet only a small percentage of peer-reviewed papers correctly employ these techniques to characterize new phosphors and prototype devices. The reluctance to transition to these advanced colorimetrics likely stems from the desire to characterize a new phosphor or prototype device with outdated techniques that would inflate the quality of optical properties rather than use modern approaches that accurately illustrate any shortcomings. There can be no progress in the design of the next-generation LED-based devices using antiquated metrics. Instead, it is up to the solid-state lighting and phosphor communities to commit to analyzing materials against these difficult-to-achieve standards. Each new material that brings us one step closer to producing high-quality light will serve as the stepping stone for new and potentially improved derivatives. Even though the data from new materials may not meet the requirements, these data can also be used in data-driven methods to uncover relationships that can further expedite new material discovery. This will further motivate the development of new luminescent materials through advanced synthetic techniques, modeling and simulations, and data-driven machine learning. Addressing these challenges is undoubtedly the only way to produce materials for the next generation of high-quality solid-state LED lighting devices.

AUTHOR INFORMATION

Corresponding Author

Jakoah Brgoch − *Department of Chemistry and the Texas Center for Superconductivity, University of Houston, Houston, Texas 77204, United States;* orcid.org/0000-0002-1406-1352; Email: jbrgoch@uh.edu

https://doi.org/10.1021/acs.inorgchem.1c02975
Inorg. Chem. 2022, 61, 4205−4218

Author

Shruti Hariyani − *Department of Chemistry and the Texas Center for Superconductivity, University of Houston, Houston, Texas 77204, United States;* orcid.org/0000-0002-4707-8863

Complete contact information is available at: https://pubs.acs.org/10.1021/acs.inorgchem.1c02975

Notes

The authors declare no competing financial interest.

Biographies

Shruti Hariyani completed her Bachelors of Science and is working on her Ph.D. in Inorganic Chemistry at the University of Houston under the supervision of Professor Jakoah Brgoch. Her research is focused on the discovery and characterization of novel phosphor materials through experiment and computation.

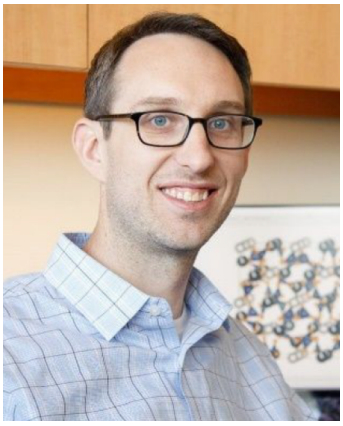

Prof. Jakoah Brgoch is an Associate Professor in the Department of Chemistry and a Principal Investigator in the Texas Center of Superconductivity where he is leading a multidisciplinary research group combining materials synthesis, characterization, first-principles computation, and machine learning. He completed his Bachelors and Masters degrees in Chemistry from Illinois State University and his Ph.D. in Chemistry from Iowa State University, following postdoctoral research at the University of California, Santa Barbara, in the Materials Research Laboratory and the Solid-State Lighting and Energy Center.

■ ACKNOWLEDGMENTS

The authors thank the National Science Foundation (Grant CER-1911311) as well as the Welch Foundation (Grant E-1981) for funding this work. This work was also supported by the Texas Center for Superconductivity at the University of Houston (TcSUH).

■ REFERENCES

(1) McFarland, E. W.; Weinberg, W. H. Combinatorial Approaches to Materials Discovery. *Trends Biotechnol.* **1999**, *17* (3), 107−115.

(2) Zenebe, D. M.; Matti, L. Investigation on Nature of Waste Heat from Incandescent Light Bulbs. *10th International Conference on Environment and Electrical Engineering*, May 8−11, 2011, Rome, Italy; Institute of Electrical and Electronics Engineers/IEEE Power & Energy Society, 2011; pp 1−4.

(3) Zukauskas, A.; Vaicekauskas, R.; Ivanauskas, F.; Gaska, R.; Shur, M. S. Optimization of White Polychromatic Semiconductor Lamps. *Appl. Phys. Lett.* **2002**, *80* (2), 234−236.

(4) U.S. Department of Energy Energy Saver. https://www.energy.gov/energysaver/led-lighting (accessed Sept 2021).

(5) Kadam, A. R.; Nair, G. B.; Dhoble, S. J. Insights into the Extraction of Mercury from Fluorescent Lamps: A Review. *J. Environ. Chem. Eng.* **2019**, *7* (4), 103279.

(6) Pust, P.; Schmidt, P. J.; Schnick, W. A Revolution in Lighting. *Nat. Mater.* **2015**, *14* (5), 454−458.

(7) George, N. C.; Denault, K. A.; Seshadri, R. Phosphors for Solid-State White Lighting. *Annu. Rev. Mater. Res.* **2013**, *43* (1), 481−501.

(8) Hermus, M.; Phan, P.-C.; Duke, A. C.; Brgoch, J. Tunable Optical Properties and Increased Thermal Quenching in the Blue-Emitting Phosphor Series: $Ba_2(Y_{1-x}Lu_x)_5B_5O_{17}:Ce^{3+}$ (x = 0 − 1). *Chem. Mater.* **2017**, *29* (12), 5267−5275.

(9) Yen, W. M.; Shinonoya, S.; Yamamoto, H. *The Phosphor Handbook*, 2nd ed.; Taylor and Francis Group: Boca Raton, FL, 2007; p 1056.

(10) Feldmann, C.; Jüstel, T.; Ronda, C. R.; Schmidt, P. J. Inorganic Luminescent Materials: 100 Years of Research and Application. *Adv. Funct. Mater.* **2003**, *13* (7), 511−516.

(11) Vitta, P.; Stanikūnas, R.; Tuzikas, A.; Reklaitis, I.; Stonkus, A.; Petrulis, A.; Vaitkevičius, H.; Žukauskas, A. *Energy-Saving Approaches to Solid State Street Lighting*; SPIE, 2011; Vol. *8123*.

(12) Ma, C.; Cao, Y.; Shen, X.; Wen, Z.; Ma, R.; Long, J.; Yuan, X. High Reliable and Chromaticity-Tunable Flip-Chip w-LEDs with Ce:YAG Glass-Ceramics Phosphor for Long-Lifetime Automotive Headlights Applications. *Opt. Mater.* **2017**, *69*, 105−114.

(13) Xie, R.-J.; Hirosaki, N.; Takeda, T. Wide Color Gamut Backlight for Liquid Crystal Displays Using Three-Band Phosphor-Converted White Light-Emitting Diodes. *Appl. Phys. Express* **2009**, *2*, 022401.

(14) Mukherjee, A.; Venkatesh, Y. V. Digital Color Reproduction on Color Television Monitors. *Comput. Gr. Image Process.* **1986**, *36* (1), 114−132.

(15) Zhuo, Y.; Brgoch, J. Opportunities for Next-Generation Luminescent Materials through Artificial Intelligence. *J. Phys. Chem. Lett.* **2021**, *12* (2), 764−772.

(16) Wang, X.-J.; Xie, R.-J. Screening and Discovery of Phosphors by the Single-Particle-Diagnosis Approach. *J. Appl. Phys.* **2021**, *129* (12), 123106.

(17) Zhuo, Y.; Mansouri Tehrani, A.; Oliynyk, A. O.; Duke, A. C.; Brgoch, J. Identifying an Efficient, Thermally Robust Inorganic Phosphor Host via Machine Learning. *Nat. Commun.* **2018**, *9* (1), 4377.

(18) Park, W. B.; Shin, N.; Hong, K.-P.; Pyo, M.; Sohn, K.-S. A New Paradigm for Materials Discovery: Heuristics-Assisted Combinatorial Chemistry Involving Parameterization of Material Novelty. *Adv. Funct. Mater.* **2012**, *22* (11), 2258−2266.

(19) Li, S.; Xia, Y.; Amachraa, M.; Hung, N. T.; Wang, Z.; Ong, S. P.; Xie, R.-J. Data-Driven Discovery of Full-Visible-Spectrum Phosphor. *Chem. Mater.* **2019**, *31* (16), 6286−6294.

(20) Ohno, Y. Spectral Design Considerations for White LED Color Rendering. *Opt. Eng.* **2005**, *44* (11), 111302.

(21) Masland, R. H. The Neuronal Organization of the Retina. *Neuron* **2012**, *76* (2), 266−280.

(22) Kaneko, A. Retinal Bipolar Cells: Their Function and Morphology. *Trends Neurosci.* **1983**, *6*, 219−223.
(23) Schmidt, T. M.; Chen, S.-K.; Hattar, S. Intrinsically Photosensitive Retinal Ganglion Cells: Many Subtypes, Diverse Functions. *Trends Neurosci.* **2011**, *34* (11), 572−580.
(24) Schnapf, J. L.; Kraft, T. W.; Baylor, D. A. Spectral Sensitivity of Human Cone Photoreceptors. *Nature* **1987**, *325* (6103), 439−441.
(25) Erdem, T.; Demir, H. V. Color Science of Nanocrystal Quantum Dots for Lighting and Displays. *Nanophotonics* **2013**, *2* (1), 57−81.
(26) Smith, T.; Guild, J. Colorimetric Standards and their Use. *Trans. Opt. Soc.* **1932**, *33* (3), 73−134.
(27) Wyman, C.; Sloan, P. P.; Shirley, P. Simple Analytic Approximations to the CIE XYZ Color Matching Functions. *J. Comput. Graph. Technol.* **2013**, *2* (2), 1−11.
(28) National Research Council. *Assessment of Advanced Solid-State Lighting*; The National Academies Press: Washington, DC, 2013.
(29) Li, S.; Wang, L.; Tang, D.; Cho, Y.; Liu, X.; Zhou, X.; Lu, L.; Zhang, L.; Takeda, T.; Hirosaki, N.; Xie, R.-J. Achieving High Quantum Efficiency Narrow-Band β-SiAlON:Eu^{2+} Phosphors for High-Brightness LCD Backlights by Reducing the Eu^{3+} Luminescence Killer. *Chem. Mater.* **2018**, *30* (2), 494−505.
(30) Zhuo, Y.; Hariyani, S.; Zhong, J.; Brgoch, J. Creating a Green-Emitting Phosphor through Selective Rare-Earth Site Preference in $NaBaB_9O_{15}$:Eu^{2+}. *Chem. Mater.* **2021**, *33* (9), 3304−3311.
(31) Denault, K. A.; George, N. C.; Paden, S. R.; Brinkley, S.; Mikhailovsky, A. A.; Neuefeind, J.; DenBaars, S. P.; Seshadri, R. A Green-Yellow Emitting Oxyfluoride Solid Solution Phosphor $Sr_2Ba(AlO_4F)_{1-x}(SiO_5)_x$:$Ce^{3+}$ for Thermally Stable, High Color Rendition Solid State White Lighting. *J. Mater. Chem.* **2012**, *22* (35), 18204−18213.
(32) Bertalmío, M. Colour Representation and Colour Gamuts. In *Vision Models for High Dynamic Range and Wide Colour Gamut Imaging*; Bertalmío, M., Ed.; Academic Press, 2020; Chapter 6, pp 131−155.
(33) Xia, Y.; Chen, J.; Liu, Y.-g.; Molokeev, M. S.; Guan, M.; Huang, Z.; Fang, M. Crystal Structure Evolution and Luminescence Properties of Color Tunable Solid Solution Phosphors $Ca_{2+x}La_{8-x}(SiO_4)_{6-x}(PO_4)_xO_2$:$Eu^{2+}$. *Dalton Trans.* **2016**, *45* (3), 1007−1015.
(34) Robertson, A. R. Computation of Correlated Color Temperature and Distribution Temperature. *J. Opt. Soc. Am.* **1968**, *58* (11), 1528−1535.
(35) Baleja, R.; Šumpich, J.; Bos, P.; Helštýnová, B.; Sokanský, K.; Novšk, T. Comparison of LED Properties, Compact Fluorescent Bulbs and Bulbs in Residential Areas. *16th International Scientific Conference on Electric Power Engineering (EPE)*, May 20−22, 2015; Kouty nad Desnou, Czech Republic; IEEE, 2015; pp 566−571.
(36) Schubert, E. F.; Kim, J. K. Solid-State Light Sources Getting Smart. *Science* **2005**, *308* (5726), 1274−1278.
(37) Li, Y. Q.; van Steen, J. E. J.; van Krevel, J. W. H.; Botty, G.; Delsing, A. C. A.; DiSalvo, F. J.; de With, G.; Hintzen, H. T. Luminescence Properties of Red-Emitting $M_2Si_5N_8$:Eu^{2+} (*M*=Ca, Sr, Ba) LED Conversion Phosphors. *J. Alloys Compd.* **2006**, *417* (1), 273−279.
(38) Brinkley, S. E.; Pfaff, N.; Denault, K. A.; Zhang, Z.; Hintzen, H. T.; Seshadri, R.; Nakamura, S.; DenBaars, S. P. Robust Thermal Performance of $Sr_2Si_5N_8$:Eu^{2+}: An Efficient Red Emitting Phosphor for Light Emitting Diode Based White Lighting. *Appl. Phys. Lett.* **2011**, *99* (24), 241106.
(39) Wang, L.; Wang, X.; Kohsei, T.; Yoshimura, K.-i.; Izumi, M.; Hirosaki, N.; Xie, R.-J. Highly Efficient Narrow-Band Green and Red Phosphors Enabling Wider Color-Gamut LED Backlight for More Brilliant Displays. *Opt. Express* **2015**, *23* (22), 28707−28717.
(40) Pust, P.; Weiler, V.; Hecht, C.; Tücks, A.; Wochnik, A. S.; Henß, A.-K.; Wiechert, D.; Scheu, C.; Schmidt, P. J.; Schnick, W. Narrow-Band Red-Emitting $Sr[LiAl_3N_4]$:Eu^{2+} as a Next-Generation LED-Phosphor Material. *Nat. Mater.* **2014**, *13*, 891−896.
(41) Soneira, R. M. Display Color Gamuts: NTSC to Rec.2020. *Inform. Display* **2016**, *32* (4), 26−31.
(42) Bechtel, H.; Czarnojan, W.; Haase, M.; Mayr, W.; Nikol, H. Phosphor Screens for Flat Cathode Ray Tubes. *Philips J. Res.* **1996**, *50* (3), 433−462.
(43) Chen, J.; Hardev, V.; Yurek, J. Quantum-Dot Displays: Giving LCDs a Competitive Edge through Color. *Inform. Display* **2013**, *29* (1), 12−17.
(44) Hase, T.; Kano, T.; Nakazawa, E.; Yamamoto, H. Phosphor Materials for Cathode-Ray Tubes. In *Advances in Electronics and Electron Physics*; Hawkes, P. W., Ed.; Academic Press, 1990; Vol. *79*, pp 271−373.
(45) Bredol, M.; Merikhi, J.; Ronda, C. Defect Chemistry and Luminescence of ZnS: Cu, Au, Al. *Ber. Bunsenges. Phys. Chem.* **1992**, *96* (11), 1770−1774.
(46) Murphy, J. E.; Garcia-Santamaria, F.; Setlur, A. A.; Sista, S. 62.4: PFS, K_2SiF_6:Mn^{4+}: the Red-Line Emitting LED Phosphor Behind GE's TriGain Technology Platform. *Dig. Tech. Pap. - Soc. Inf. Disp. Int. Symp.* **2015**, *46* (1), 927−930.
(47) Van der Heggen, D.; Joos, J. J.; Smet, P. F. Importance of Evaluating the Intensity Dependency of the Quantum Efficiency: Impact on LEDs and Persistent Phosphors. *ACS Photonics* **2018**, *5* (11), 4529−4537.
(48) Zhao, M.; Liao, H.; Ning, L.; Zhang, Q.; Liu, Q.; Xia, Z. Next-Generation Narrow-Band Green-Emitting $RbLi(Li_3SiO_4)_2$:Eu^{2+} Phosphor for Backlight Display Application. *Adv. Mater.* **2018**, *30* (38), 1802489.
(49) Rizzo, P.; Rea, M.; White, R. Lighting for Today's Neonatal Intensive Care Unit. *Newborn Infant Nurs. Rev.* **2010**, *10* (2), 107−113.
(50) Davis, W.; Ohno, Y. Color Quality Scale. *Opt. Eng.* **2010**, *49* (3), 033602.
(51) Yuen, G. S. c.; Sproul, A. B.; Dain, S. J. Performance of 'Energy Efficient' Compact Fluorescent Lamps. *Clin. Exp. Optom.* **2010**, *93* (2), 66−76.
(52) Piao, X.; Machida, K.-i.; Horikawa, T.; Yun, B. Acetate Reduction Synthesis of $Sr_2Si_5N_8$:Eu^{2+} Phosphor and its Luminescence Properties. *J. Lumin.* **2010**, *130* (1), 8−12.
(53) Sun, L.; Devakumar, B.; Liang, J.; Wang, S.; Sun, Q.; Huang, X. A Broadband Cyan-Emitting $Ca_2LuZr_2(AlO_4)_3$:Ce^{3+} Garnet Phosphor for Near-Ultraviolet-Pumped Warm-White Light-Emitting Diodes with an Improved Color Rendering Index. *J. Mater. Chem. C* **2020**, *8* (3), 1095−1103.
(54) Horikawa, T.; Piao, X. Q.; Fujitani, M.; Hanzawa, H.; Machida, K. Preparation of $Sr_2Si_5N_8$:Eu^{2+} Phosphors Using Various Novel Reducing Agents and their Luminescent Properties. *IOP Conf. Ser.: Mater. Sci. Eng.* **2009**, *1*, 012024.
(55) Driel, W. D. v.; Fan, X.; Zhang, G. Q. *Solid State Lighting Reliability*; Springer: Cham, Switzerland, 2018; Part 2, p 606.
(56) Krames, M. R.; Shchekin, O. B.; Mueller-Mach, R.; Mueller, G. O.; Zhou, L.; Harbers, G.; Craford, M. G. Status and Future of High-Power Light-Emitting Diodes for Solid-State Lighting. *J. Disp. Technol.* **2007**, *3* (2), 160−175.
(57) Park, K.; Kim, T.; Yu, Y.; Seo, K.; Kim, J. Y/Gd-Free Yellow $Lu_3Al_5O_{12}$:Ce^{3+} Phosphor for White LEDs. *J. Lumin.* **2016**, *173*, 159−164.
(58) Zhou, Y.; Zhuang, W.; Hu, Y.; Liu, R.; Xu, H.; Chen, M.; Liu, Y.; Li, Y.; Zheng, Y.; Chen, G. Cyan-Green Phosphor $(Lu_2M)(Al_4Si)O_{12}$:Ce^{3+} for High-Quality LED Lamp: Tunable Photoluminescence Properties and Enhanced Thermal Stability. *Inorg. Chem.* **2019**, *58* (2), 1492−1500.
(59) Ohno, Y. *Color Rendering and Luminous Efficacy of White LED Spectra*; SPIE, 2004; Vol. *5530*.
(60) Huang, P.; Zhao, Y.; Wang, J.; Zheng, Y.; Yang, P.; Zheng, Q.; Gu, S.; Zhou, B.; Jiang, W.; Wang, L. Tunable Chromaticity and High Color Rendering Index of WLEDs with $CaAlSiN_3$:Eu^{2+} and YAG:Ce^{3+} Dual Phosphor-in-Silica-Glass. *J. Am. Ceram. Soc.* **2020**, *103* (9), 4989−4998.

https://doi.org/10.1021/acs.inorgchem.1c02975
Inorg. Chem. 2022, 61, 4205−4218

(61) Setlur, A. A.; Radkov, E. V.; Henderson, C. S.; Her, J.-H.; Srivastava, A. M.; Karkada, N.; Kishore, M. S.; Kumar, N. P.; Aesram, D.; Deshpande, A.; Kolodin, B.; Grigorov, L. S.; Happek, U. Energy-Efficient, High-Color-Rendering LED Lamps Using Oxyfluoride and Fluoride Phosphors. *Chem. Mater.* **2010**, *22* (13), 4076−4082.
(62) Lv, L.; Jiang, X.; Huang, S.; Chen, X. a.; Pan, Y. The Formation Mechanism, Improved Photoluminescence and LED Applications of Red Phosphor K_2SiF_6:Mn^{4+}. *J. Mater. Chem. C* **2014**, *2* (20), 3879−3884.
(63) Zhu, H.; Lin, C. C.; Luo, W.; Shu, S.; Liu, Z.; Liu, Y.; Kong, J.; Ma, E.; Cao, Y.; Liu, R.-S.; Chen, X. Highly Efficient Non-Rare-Earth Red Emitting Phosphor for Warm White Light-Emitting Diodes. *Nat. Commun.* **2014**, *5* (1), 4312.
(64) Hariyani, S.; Brgoch, J. Advancing Human-Centric LED Lighting Using Na_2MgPO_4F:Eu^{2+}. *ACS Appl. Mater. Interfaces* **2021**, *13* (14), 16669−16676.
(65) Ohno, Y. CIE Fundamentals for Color Measurements. *NIP & Digital Fabrication Conference* **2000**, *2000* (2), 540−545.
(66) Kim, J. S.; Park, Y. H.; Kim, S. M.; Choi, J. C.; Park, H. L. Temperature-Dependent Emission Spectra of M_2SiO_4:Eu^{2+} (*M*=Ca, Sr, Ba) Phosphors for Green and Greenish White LEDs. *Solid State Commun.* **2005**, *133* (7), 445−448.
(67) Jennifer, D. T. K. *Field Guide to Colorimetry and Fundamental Color Modeling*; Society of Photo-Optical Instrumentation Engineers (SPIE): Bellingham, WA, 2018.
(68) Lou, S.; Gong, C.; Wu, N.; Xu, Z. Power Optimization Under Brightness and Communication Requirements for Visible Light Communication Based on MacAdam Ellipse. *J. Commun. Netw.* **2017**, *2* (4), 28−35.
(69) Narendran, N.; Deng, L.; Pysar, R.; Gu, Y.; Yu, H. *Performance Characteristics of High-Power Light-Emitting Diodes*; SPIE, 2004; Vol. *5187*.
(70) Weatherall, I. L.; Coombs, B. D. Skin Color Measurements in Terms of CIELAB Color Space Values. *J. Invest. Dermatol.* **1992**, *99* (4), 468−473.
(71) Hanbury, A.; Serra, J. Mathematical Morphology in the CIELAB Space. *Image Anal. Stereol.* **2002**, *21* (3), 201.
(72) Kumada, J.; Nishizawa, T. Reproducible Color Gamut of Television Systems. *J. SMPTE* **1992**, *101* (8), 559−564.
(73) Li, J.-S.; Lai, C.-C.; Hsu, C.-F.; Chang, T.-Y.; Wang, W.-C. P-37: Color Reproduction Method of Adobe RGB Images on Wide Color Gamut Display. *Dig. Tech. Pap. - Soc. Inf. Disp. Int. Symp.* **2009**, *40* (1), 1227−1230.
(74) Yoshimura, K.; Fukunaga, H.; Izumi, M.; Takahashi, K.; Xie, R.-J.; Hirosaki, N. Achieving Superwide-Color-Gamut Display by Using Narrow-Band Green-Rmitting γ-AlON:Mn,Mg Phosphor. *Jpn. J. Appl. Phys.* **2017**, *56* (4), 041701.
(75) Yu, H.; Wang, B.; Bu, X.; Liu, Y.-g.; Chen, J.; Huang, Z.; Fang, M. A Facile In Situ Surface-Coating Passivation Strategy for Improving the Moisture Resistance of Mn^{4+}-Activated Fluoride Red Phosphor. *Ceram. Int.* **2020**, *46* (11), 18281−18286.
(76) Wang, X.; Takeda, T.; Hirosaki, N.; Funahashi, S.; Xie, R.-J. Single-Particle-Diagnosis Approach: An Efficient Strategy for Discovering New Nitride Phosphors. *J. Rare Earths* **2018**, *36* (1), 42−48.
(77) Duke, A. C.; Hermus, M.; Brgoch, J. Structure Transformation and Cerium-Substituted Optical Response across the Carbon-itridosilicate Solid Solution $(La_\delta Y_{1-\delta})_2Si_4N_6C$ (δ = 0−0.5). *Inorg. Chem.* **2018**, *57* (1), 519−527.
(78) Zhong, Y.; Xia, M.; Chen, Z.; Gao, P.; Hintzen, H. T.; Wong, W.-Y.; Wang, J.; Zhou, Z. Pyrophosphate Phosphor Solid Solution with High Quantum Efficiency and Thermal Stability for Efficient LED Lighting. *iScience* **2020**, *23* (3), 100892.
(79) Barai, V. L.; Dhoble, S. J. Prediction of Excitation Wavelength of Phosphors by Using Machine Learning Model. *J. Lumin.* **2019**, *208*, 437−442.
(80) Li, S.; Xie, R.-J. Critical Review—Data-Driven Discovery of Novel Phosphors. *ECS J. Solid State Sci. Technol.* **2020**, *9* (1), 016013.
(81) Li, M.; Zhang, X.; Zhang, H.; Chen, W.; Ma, L.; Wang, X.; Liu, Y.; Lei, B. Highly Efficient and Dual Broad Emitting Light Convertor: An Option for Next-Generation Plant Growth LEDs. *J. Mater. Chem. C* **2019**, *7* (12), 3617−3622.
(82) Salehi, A.; Fu, X.; Shin, D.-H.; So, F. Recent Advances in OLED Optical Design. *Adv. Funct. Mater.* **2019**, *29* (15), 1808803.

https://doi.org/10.1021/acs.inorgchem.1c02975
Inorg. Chem. 2022, 61, 4205−4218